ROYAL SOCIETY OF CHEMISTRY

COMMUNICATION

Check for updates

Self-assembled Janus plasmene nanosheets as flexible 2D photocatalysts†

Runfang Fu, [ID] [a] Qianqian Shi,*[a] Zijun Yong,[a] James C. Griffith, [ID] [b] Lim Wei Yap [ID] [a] and Wenlong Cheng [ID] *[a]

A leaf is a free-standing photocatalytic system that can effectively harvest solar energy and convert CO_2 and H_2O into carbohydrates in a continuous manner without the need for regeneration or tedious product extraction steps. Despite encouraging advances achieved in designing artificial photocatalysts, most of them function in bulk solution or on rigid surfaces. Here, we report on a 2D flexible photocatalytic system based on close packed Janus plasmene nanosheets. One side of the Janus nanosheets is hydrophilic with catalytically active palladium, while the opposite side is hydrophobic with plasmonic nanocrystals. Such a unique design ensures a stable nanostructure on a flexible polymer substrate, preventing dissolution/degradation of plasmonic photocatalysts during chemical conversion in aqueous solutions. Using catalytic reduction of 4-nitrophenol as a model reaction, we demonstrated efficient plasmon-enhanced photochemical conversion on our flexible Janus plasmene. The photocatalytic efficiency could be tuned by adjusting the palladium thickness or types of constituent building blocks or their orientations, indicating the potential for tailor-made catalyst design for desired reactions. Furthermore, the flexible Janus plasmene nanosheets were designed into a small 3D printed artificial tree, which could continuously convert 30 mL of chemicals in 45 minutes.

Solar energy is a clean, abundant and sustainable energy source. In nature, plant foliage works as an excellent sunlight harvester that captures solar energy to realize the conversion of water and carbon dioxide (CO_2) into carbohydrates and oxygen (O_2). This natural process stimulates the development of a series of photocatalysts which could utilize energy of photons

New concepts

We demonstrate a unique 2D flexible photocatalyst based on close packed Janus plasmene nanosheets. Such Janus plasmene nanosheets intimately integrated light-absorbing plasmonic and catalytically active materials into one system and thus worked as both a sunlight harvester and catalyst for the reduction of 4-nitrophenol (4-NP). The flexible control over the plasmonic building blocks further allows an adjustable absorption range of the catalysts for efficient utilization of solar energy. Particularly, the Janus plasmene nanosheets distinctively feature one hydrophilic side with palladium and one hydrophobic side protected by entangled polymeric ligands. This distinct characteristic endows structural and catalytic stability in aqueous solution without dissolution or degradation of the photocatalysts and further allows a continuous catalytic reaction. Such stability and recyclability are distinguishable from present plasmonic nanostructure-based catalysts that are mostly bulk solution-based with low catalytic stability and need tedious regeneration processes. As a proof of concept, an "artificial tree" was built by using the Janus plasmene nanosheets which can effectively realize 30 mL-chemical conversion under sunlight irradiation. Our present design of Janus plasmene nanosheets indicates potential application in customizing 2D flexible photocatalysts for sustainable solar-to-chemical conversion.

to drive many useful chemical reactions for solar fuel production, decomposition of pollutants, and self-cleaning products.[1] One important prerequisite for solar to chemical energy conversion is to develop photocatalysts with a high efficiency of solar energy harvesting and the ability to drive chemical reactions in the range of the solar spectrum, especially the visible to near-infrared (NIR) region.[2,3] Among various photocatalysts, plasmonic nanostructures show great potential in the efficient utilization of solar energy to drive chemical reactions. The unique localized surface plasmon resonance (LSPR) of plasmonic nanostructures covers a broad range from ultraviolet (UV) to near-infrared (NIR) due to the interaction between light and free electrons on the metal surface.[4–6]

It has been reported that the LSPR of plasmonic nanostructures has been successfully applied in facilitating the efficient conversion of solar energy to chemical energy.[7,8] For instance,

[a] *Department of Chemical Engineering, Faculty of Engineering, Monash University, Clayton 3800, Victoria, Australia. E-mail: wenlong.cheng@monash.edu, qianqian.shi@monash.edu*

[b] *Monash X-ray Platform, Monash University, Clayton 3800, Victoria, Australia*

† Electronic supplementary information (ESI) available: Experimental section. Detailed characterization of Janus plasmonic nanoparticles and plasmenes; optical properties of Janus plasmenes; catalytic performance of control samples (Fig. S1–S19). Catalytic performance of an artificial tree (Supplementary video). See DOI: 10.1039/d0mh01275k

bimetallic nanoparticles that consist of plasmonic and catalytic metals including (gold core)@(ceria shell) nanostructures,[3] Au/Pd@mesoporous SiO$_2$ yolk–shell hetero-nanostructures,[9] a Au/Pt bimetallic grating,[10] Au/Ag core/shell nanorods,[11] Au NP-Pd/Ag nanoshell dimers,[12] and Pd-modified Au nanorods[13] could effectively harvest visible light to enhance the catalytic performance in oxidation reactions,[14,15] coupling reactions[12,16,17] or catalytic degradation of pollutants.[11,18] The effective absorption of solar energy by plasmonic nanostructures could even allow a lower operating temperature in some of the conventional oxidation reactions that normally run at high temperature.[14] However, the catalytic performance of these plasmonic nanocolloids could be drastically degraded by the small molecules or polymeric ligands which are used to ensure their stability in bulk solution.[19,20] Furthermore, additional separation processes are normally needed to recycle the catalytic nanoparticles, resulting in possible irreversible aggregation of catalysts.

Inspired by the continuous photosynthesis enabled by natural leaves, here we designed a 2D flexible photocatalyst from Janus plasmene nanosheets to addresss the above challenges. Such Janus plasmene nanosheets intimately integrated light-absorbing plasmonic and catalytically active materials into one system and thus worked as both a sunlight harvester and catalyst for the reduction of 4-nitrophenol (4-NP). The flexible control over the plasmonic building blocks further allows us to tune the absorption range of the catalysts for efficient utilization of solar energy. It is worthy of note that the as-designed 2D structure distinctively featured one hydrophilic side with catalytically active Pd and one hydrophobic side protected by entangled polymeric ligands. Thus, it showed excellent structural and catalytical stability in aqueous solution without dissolution or degradation of the plasmonic photocatalysts from the substrate. As a proof of concept, we designed an "artificial leaf" by conformally immobilizing our ultrathin and soft Janus plasmene nanosheet on a flexible polymer substrate

and further assembled them into a 3D printed "artificial tree" which could realize an effective conversion from solar energy to chemical energy in a continuous manner.

Results and discussion

Fabrication of Janus plasmene nanosheets

We began with the fabrication of 2D plasmene nanosheets through a two-step drying-mediated self-assembly method using gold nanocubes (Au NCs) as the model building block.[21] In brief, the Au NC nanoparticles were firstly functionalized with thiol-terminated polystyrene (SH-PS) via a ligand exchange method.[22] The ultrathin 2D plasmene nanosheets (Fig. 1a) were then formed on a Si wafer by a drying-mediated air–water interface self-assembly process. Cross-section (Fig. 1b) and top-view (Fig. 1c) scanning electron microscopy (SEM) images confirmed a highly ordered, closed-packed and one-particle thick structure of the obtained 2D plasmene.

To fabricate the Janus plasmene nanosheets, we adopted our recently developed ligand symmetry breaking approach.[23] Taking advantage of the "masking" effect from the substrate (Si wafer), we could selectively expose one side of the Au NC surfaces (Fig. 1d) by removing PS from the air-facing side through air plasma treatment. SEM images indicate that there is no obvious destruction of the structures of the plasmene nanosheets (Fig. 1e and f). The exposed Au NC surfaces then served as the site for the deposition of catalytic palladium (Pd) (Fig. 1g).[24] Fig. 1h and i show that Pd was preferentially deposited on the exposed Au NC surface, giving an asymmetric structure. Transmission electron microscopy (TEM) and scanning transmission electron microscopy (STEM)-energy-dispersive X-ray spectroscopy (EDX) images (Fig. 1j–m and Fig. S1, ESI†) further confirmed the Janus morphology and compositional distribution on different sides of the as-prepared 2D plasmene nanosheets.
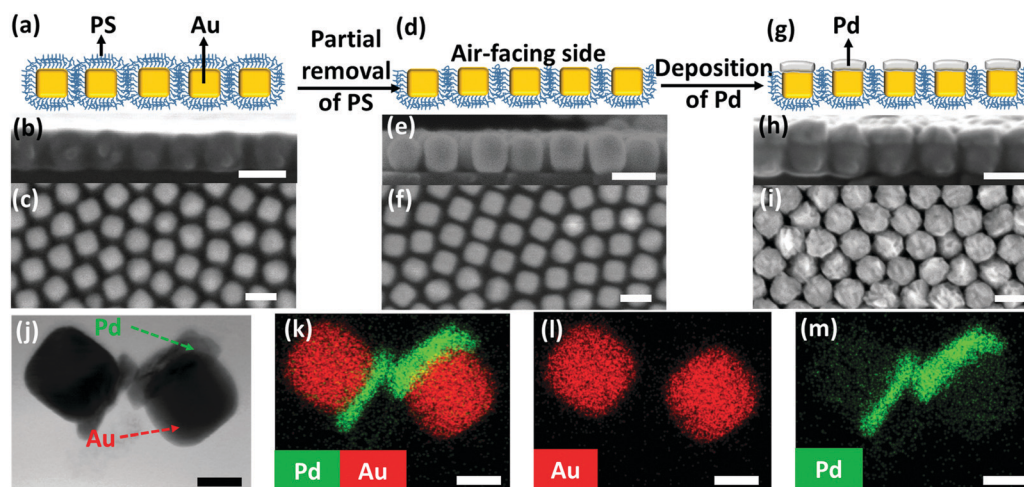

Fig. 1 Fabrication of Janus plasmene nanosheets. (a, d, and g) Scheme of fabricating Janus plasmene nanosheets. Cross-section SEM image of (b) PS-capped, (e) one-side exposed and (h) Janus plasmene nanosheets on a Si wafer and (c, f, and i) their corresponding top-view SEM images. (j) Dark-field TEM images of individual Janus NPs and (k–m) corresponding EDX elemental mapping images (red: Au; green: Pd). (Scale bar: 50 nm for SEM, 20 nm for TEM.)

X-ray photoelectron spectroscopy (XPS) has also been carried out to analyse the compositions of such Janus plasmene nanosheets. As can be seen in the high-resolution Au 4f region scans for the original plasmene nanosheets (Fig. S2, ESI†), the Au $4f_{7/2}$ peak located at a binding energy (BE) value of 84.2 eV was observed with the Au $4f_{5/2}$ spin orbit splitting component at 87.8 eV.[25] For the Janus plasmene (Fig. S3a, ESI†), besides the Au $4f_{7/2}$ peak that is located at a BE value of 84.4 eV with the Au $4f_{5/2}$ spin orbit splitting component at 88.1 eV, the broad Pd 4s peak located at 87.4 eV[26] obviously shows up and makes a considerable contribution to the spectral envelope in the Au 4f region. Additionally, the overlapping Pd loss features and the characteristic Pd 3d metallic peaks located at 335.3 eV (Pd $3d_{5/2}$) and 340.6 eV (Pd $3d_{3/2}$) with a doublet separation of 5.26 eV[26] evidently demonstrate the existence of the Pd component in the Janus plasmene (Fig. S3b, ESI†).

It is worth mentioning that the PS ligand plays an important role in our unique leaf-like design by using 2D Janus plasmene nanosheets. In the self-assembly stage, PS could guarantee the formation of a monolayered structure by regulating the inter-particle forces.[27] In the stage of forming Janus nanosheets, its intrinsic hydrophobicity largely slows down the contact of the growth solution with the protected Au surface and thus allows for the selective deposition of Pd on one side of the nanosheet.

To further prove this, we applied the same experimental process to CTAB-capped Au NCs sitting on a Si wafer (Fig. S4a, ESI†). The results showed an isotropic coating of Pd on all surfaces of the Au NC rather than a selective deposition on one side (Fig. S4b, ESI†). Most importantly, the entanglement of PS helps to maintain the structural integrity of the nanosheet in the aqueous solution where the deposition of Pd and the catalytic reaction take place. This integrity leads to a stable leaf mimicking structure on a flexible polymeric substrate for continuous conversion of solar to chemical energy.

Plasmon-enhanced catalytic performance

To characterize the photocatalytic performances of our 2D Janus plasmenes, we choose the catalytic reduction of 4-NP by sodium borohydride ($NaBH_4$) as the model reaction. This reaction process can be monitored either by the colour change or the absorption peak change of the reactants.[18,20,28,29] The yellowish colour of 4-NP gradually disappeared upon the addition of the 2D Janus plasmene, which indicates the successful conversion of the reactant (Fig. 2a). Spectroscopy characterization showed that the absorption peak of 4-NP at 400 nm gradually weakened and a new peak at 300 nm simultaneously appeared with increasing intensity, demonstrating the successful conversion of 4-NP to 4-aminophenol (4-AP) (Fig. 2a).
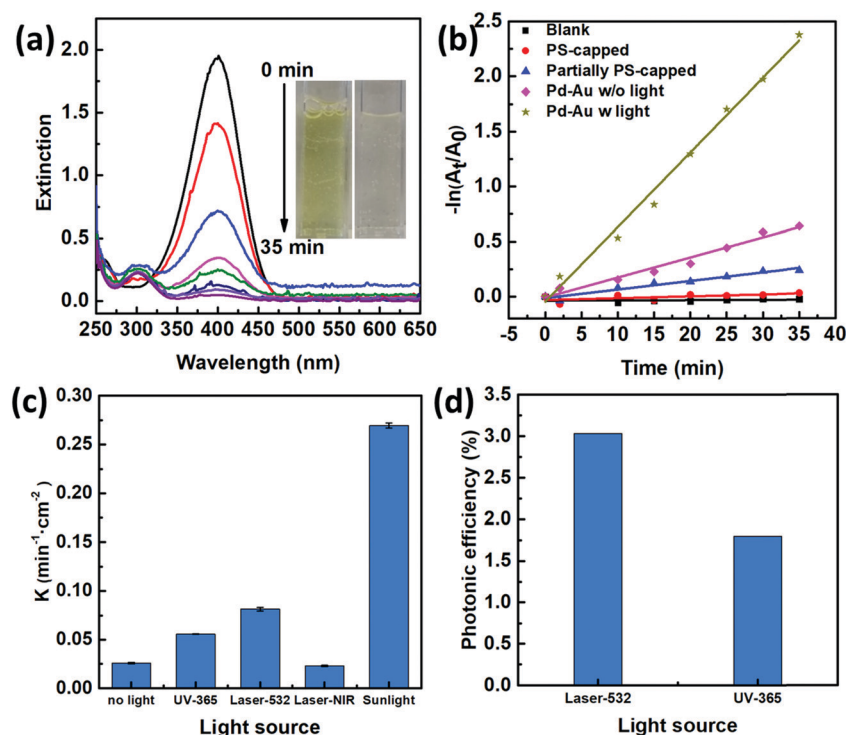

Fig. 2 Photocatalytic properties of Janus plasmene nanosheets under various conditions. (a) The evolution of the UV-vis spectra of the catalytic reaction solution during the reduction of 4-NP to 4-AP (the inserts are the photos of the solution before (top) and after (bottom) the reaction). (b) The relationship between $-\ln(A_t/A_0)$ and the reaction time from different plasmene nanosheets: PS-capped plasmene nanosheets with sunlight irradiation (red curve), partially PS-capped plasmene nanosheets with sunlight irradiation (blue curve), Pd–Au Janus plasmene nanosheets without sunlight irradiation (pink curve) and Pd–Au Janus plasmene nanosheets with sunlight irradiation (dark yellow curve). A_t and A_0 are the absorbance at fixed intervals and the initial state of the UV-vis spectra, respectively. (The black curve is the control experiment without plasmene nanosheets.) (c) Catalytic rate (normalized to the geometric surface area of the plasmene) of Pd–Au Janus plasmene nanosheets under different light irradiation. (d) The photonic efficiency under laser-532 and UV-365 irradiation.

We compared the kinetic curves of the reduction reaction from three different nanosheets (Fig. 2b). When no catalyst was added, no reduction reaction was observed even after sunlight irradiation of 35 min (Fig. 2b, black curve). This result indicates that catalysts are required in our system to overcome the kinetic barrier between the mutually repelling electrons of 4-NP and NaBH$_4$.[30] We also found that the exposed area of the Au NC had a direct impact on the catalytic performance. The PS-capped Au NC-based nanosheets show almost no catalytic performance under sunlight (Fig. 2b, red curve), which was presumably due to the intrinsic hydrophobicity of PS preventing the reaction solution from interacting with the catalyst. When increasing the exposed area by partially removing the PS ligands, the catalytic rate was evidently improved (Fig. 2b, blue curve). Such experimental results were consistent with the poisoning effect of ligands on metallic nanoparticles in other work.[19,20] We further investigated the influence of scavengers on the catalytic kinetics by using methanol and acetone as hole and electron scavengers,[31,32] respectively (Fig. S5, ESI†). Clearly, the addition of acetone had a more significant effect on slowing down the reaction kinetics, demonstrating an electron-dominant catalytic mechanism.

Among all the samples, the Janus nanosheet showed the highest catalytic performance (Fig. 2b). The catalytic rate (k = 0.27 min^{-1} cm^{-2}) of the Janus 2D plasmene nanosheets with sunlight (Fig. 2b, dark yellow curve) is ~4 times higher than that without sunlight (Fig. 2b, pink curve, 0.07 min^{-1} cm^{-2}). This indicates that the plasmonic effect contributes largely to the enhancement of the catalytic reduction under sunlight irradiation. Gold nanoparticles have been demonstrated to serve as a light harvester that can capture light energy to improve catalytic reactions.[12,33] It has been hypothesized that two effects from the excitation of surface plasmons possibly contribute to the enhancement of reactions:[14,34] one is the heating effect generated by the energetic electrons relaxing and another one is the transfer of energetic electrons to adsorbates, which leads to activated molecules on the surface of plasmonic nanostructures. In our case, the catalytic reduction of 4-NP could be enhanced by thermal heating (Fig. S6, ESI†). Thus, the Au NC-based plasmene that was excited by sunlight possibly helped to enhance the catalytic activity by photothermal effects (Fig. S7, ESI†) and/or hot electron effects promoting electron transfer to 4-NP.[35,36] In contrast, the pure Pd NC-based nanosheets without the plasmonic component didn't show obvious enhancement in the catalytic performance under the same experimental conditions (Fig. S8, ESI†). Furthermore, the catalytic performance of the Janus plasmene nanosheets (Fig. 2b, dark yellow curve) was about 9 times that of the pure Au NC nanosheets (Fig. 2b, blue curve) and pure Pd NC-based nanosheets (Fig. S8, ESI†, red curve) under sunlight irradiation. Such enhancement is more significant than previous Au@Ag core–shell systems,[20,37] demonstrating the attributes of our Janus structural design.

We further investigated the photo-enhanced catalytic performance under various light sources as shown in Fig. 2c. As expected, sunlight has broadband excitation, hence exhibiting the highest catalytic rate. Further comparisons at particular wavelengths showed that the laser at 532 nm gave the highest rate. This may be due to the fact that this wavelength is close to the plasmon resonance peak of the Janus plasmene (~580 nm, Fig. S9, ESI†).

We further compared the photonic efficiency[38] (ξ) of monochromatic light of 365 nm and 532 nm by using the following equations:

$$\xi(\%) = N_m/N_p \times 100 \quad (1)$$

$$N_p = (I \times S \times \lambda)/hc \quad (2)$$

where N_m is the number of degraded molecules per second, N_p is the number of absorbed photons per second, I is the intensity of light (W cm^{-2}), S is the irradiated surface area (cm^2), λ is the wavelength of light, h is the Planck constant (6.63 × 10^{-34} J s) and c is the speed of light (3 × 10^8 m s^{-1}). As shown in Fig. 2d, the photonic efficiency under 532 nm irradiation was estimated to be ~3.0%, which is much higher than that under 365 nm irradiation (~1.8%). This demonstrates the significance of plasmon resonance in enhancing the catalytic efficiency.

The effect of the catalytic component on the plasmon-enhanced catalytic performance

To better ascertain the effect of the catalytic component (Pd) on the plasmon-enhanced catalytic property, we finely tune the Pd thicknesses of the Janus plasmene nanosheets from ~6 to ~17 nm by increasing the concentration of the Pd precursor from 0.1 mM to 1.0 mM (Fig. 1g–j, 3a, and Fig. S10, ESI†). The reaction rate k of the Janus plasmene nanosheets firstly increased and then decreased with increasing Pd thickness (Fig. 3b). A maximum value was obtained at a thickness of ~14 nm in our studies. It has been reported that, in the Au–Pd catalytic system, the balance between the number of active sites and the ease of product desorption plays a key role in the catalytic activity.[39] Such balance has been proved to be sensitive to the content of Pd. We found that Pd was deposited on the surface of Au NCs with a speckle-like shape at a low concentration of the Pd precursor (Fig. S10a, ESI†), which might lead to slow adsorption of 4-NP and further result in a low rate constant (k = 0.04 min^{-1} cm^{-2} without light and k = 0.06 min^{-1} cm^{-2} with sunlight). With increasing concentration of the Pd precursor, Pd gradually covered the exposed surface of the Au NCs (Fig. S10b–d, ESI† and Fig. 1i), giving increased adsorption of reactants. However, the binding energy between the reaction product and the catalysts was increased meanwhile.[39] Thus, when the Pd thickness was further increased from ~14 nm to ~17 nm (Fig. 3b), we observed decreasing catalytic rates from 0.10 min^{-1} cm^{-2} to 9.6 × 10^{-2} min^{-1} cm^{-2} without sunlight and from 0.16 min^{-1} cm^{-2} to 0.15 min^{-1} cm^{-2} with sunlight.

Importantly, the catalytic rates of the Janus plasmene nanosheets with sunlight are always higher than those without sunlight, regardless of the Pd thickness. This result indicates that the plasmonic component in the Janus plasmene nanosheets contributes largely to the catalytic reduction of 4-NP
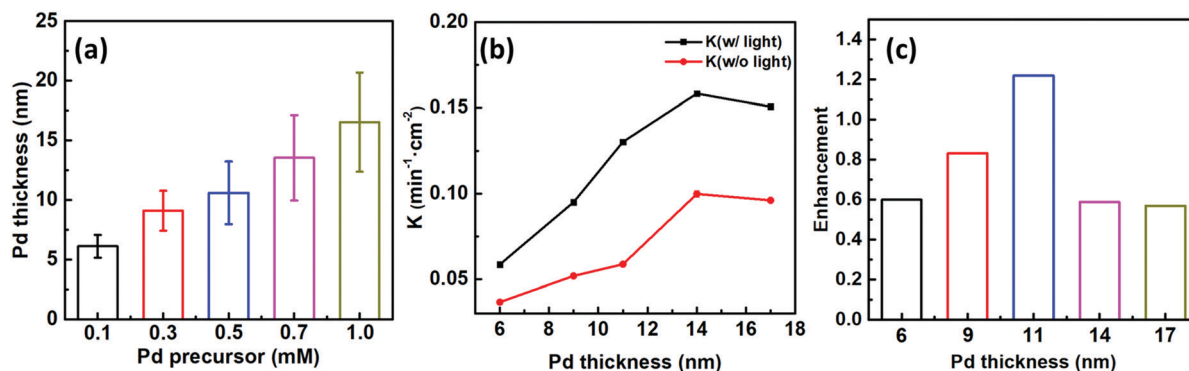
Fig. 3 The effect of the Pd thickness on the plasmon-enhanced catalytic property of the Janus plasmene nanosheets. (a) Thickness change of Pd on Au NC nanosheets with increasing concentration of the Pd precursor. (b) Catalytic rate (normalized to the geometric surface area of the plasmene) of Janus plasmene nanosheets with different Pd thicknesses w/light (black curve) and w/o light (red curve) and (c) their corresponding plasmon enhancement.

under sunlight irradiation. To quantify the plasmon-enhanced effect in the catalytic reaction, the enhancement (E) is calculated by the following eqn (3):

$$E = \frac{k(\text{w/light}) - k(\text{w/o light})}{k(\text{w/o light})} \quad (3)$$

where k (w/light) is the catalytic rate with sunlight, and k (w/o light) is the catalytic rate without sunlight. We found that the thickness of Pd could lead to an obvious influence on the plasmon resonance peak position (Fig. S11, ESI†). When the Pd thickness increased from ~6 nm to ~17 nm, the plasmon resonance peak blue shifted ~3 nm to ~15 nm (Fig. S12, ESI†), indicating a weakened plasmonic coupling effect. This increased blue shift demonstrates a possible damping effect of Pd on the plasmon resonance of the Au plasmene, which also has been observed in other Pd–Au nanostructures.[2,40,41] Fig. 3c shows that the enhancement increases firstly as the Pd becomes thicker and reaches the highest value (~1.2) when the Pd thickness is about 11 nm and then decreases with further increasing Pd thickness. This kind of evolution trend is likely due to the balance between the increasing plasmon damping effect of Pd and the active sites. As discussed above, the increasing Pd thickness might enhance the absorption of 4-NP molecules on the surface of the Janus plasmene, thus leading to more activated 4-NP molecules by the energetic electrons generated from the excited plasmene and giving increased enhancement. However, a further increase of the Pd thickness resulted in a dominant effect from plasmon damping of Pd and the increase of the binding energy between 4-AP and the plasmene, leading to the decreased enhancement.

The effect of the plasmonic component on the plasmon-enhanced catalytic performance

One attribute of our flexible Janus plasmene leaf is that we can finely tune the sizes, shapes and even orientations of the building blocks to engineer the desired light–matter interactions in a broadband spectral window.[42–44] To illustrate this, we chose Au nanobipyramids (Au NBPs) as another building block due to their unique geometry- and orientation-dependent plasmonic properties.[43,45] By adjusting the length of the PS

ligands, we could obtain horizontally-aligned Au NBP-based (H-NBPs, Fig. S13a, ESI†) and vertically-aligned Au NBP-based (V-NBPs, Fig. S13b, ESI†) plasmene nanosheets, which were then used to fabricate Janus Au–Pd plasmene nanosheets following the same protocol as described above for NC-based Janus plasmene nanosheets. The exposed Au surface could selectively be the side or the tip of Au NBPs depending on the alignment of the Au NBPs. Exposing the side of Au NBPs for Pd deposition using H-NBPs leads to side-coated Au NBPs (Fig. 4a and Fig. S13c, ESI†). The TEM (Fig. 4a) and elemental mapping (Fig. S14a and b, ESI†) results confirmed a Pd layer with a thickness of ~13 nm, a width of ~24 nm and a length of ~53 nm only on one side of the Au NBPs. Alternatively, tip-Pd-coated Au NBPs were obtained by selectively exposing one tip of V-NBPs (Fig. 4b and Fig. S13d, ESI†), which showed a Pd thickness of ~15 nm and a width of ~20 nm only on one tip of the Au NBPs (Fig. 4b and Fig. S14c and d, ESI†). Similar to the previous NC-based Janus plasmene, the XPS results further evidently confirm the Pd and Au composition in NBP plasmenes (Fig. S15, ESI†).

Fig. 4c indicates that both H-NBP and V-NBP Janus plasmene nanosheets show enhanced catalytic performance under sunlight irradiation. In particular, we found that the enhancement of H-NBP Janus plasmene nanosheets (~1.7) is around 2 times of that of V-NBP Janus plasmene nanosheets (~0.9) (Fig. 4d). This might be attributed to a broader absorption peak of H-NBP plasmene nanosheets in comparison with V-NBP plasmene nanosheets, which show a predominant absorption peak at around 570 nm (Fig. S16, ESI†). As a result, the broad light absorption might endow the H-NBP Janus plasmene nanosheets with a high efficiency of light harvesting and thus a high enhancement in catalytic activity.

Artificial tree

In addition to the Janus morphologies, our Au–Pd nanosheets also possess distinct surface chemistry with the Pd side being hydrophilic, whereas the Au side is hydrophobic (Fig. S17, ESI†). Such "surfactant-like" structures allow our Janus nanosheets to be readily accessible to aqueous reactants on
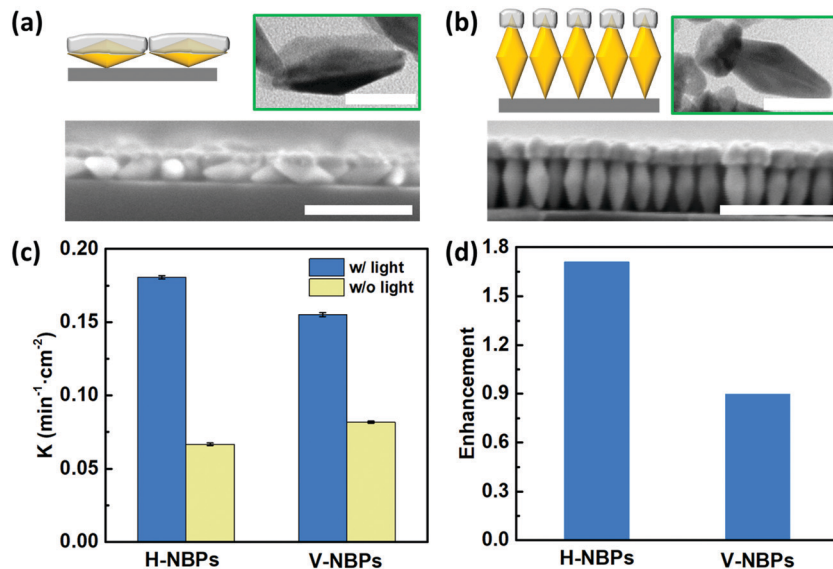
Fig. 4 Controlling the plasmon-enhanced catalytic property by tuning the alignment of plasmonic NPs. Scheme (top left) and cross-section SEM image (bottom) of (a) H-NBP and (b) V-NBP Janus plasmene nanosheets, top right is the corresponding TEM images of an individual Janus NP. (c) The comparison of the reduction rate (normalized to the geometric surface area of the plasmene) between H-NBP and V-NBP Janus plasmene nanosheets w/and w/o light irradiation. (d) The comparison of the plasmon enhancement between Pd-H-NBP and Pd-V-NBP Janus plasmene nanosheets. (Scale bar for TEM: 50 nm, SEM: 100 nm.)

their hydrophilic faces (*i.e.* Pd sides) and simultaneously maintain structural integrity without dissolution or degradation due to hydrophobic PS ligand protection.

Such unique structural and functional features motivated us to design an artificial leaf to mimic the continuous reaction in a natural system. To demonstrate this, we fabricated a polymeric tree (~15 mm in width and ~25 mm in height) by mounting 8 pieces of "artificial leaves" onto branches of a 3D-printed tree (Fig. 5a). As shown in Fig. 5a–d, our 2D Janus plasmene nanosheets are similar to the light harvesting photosynthetic
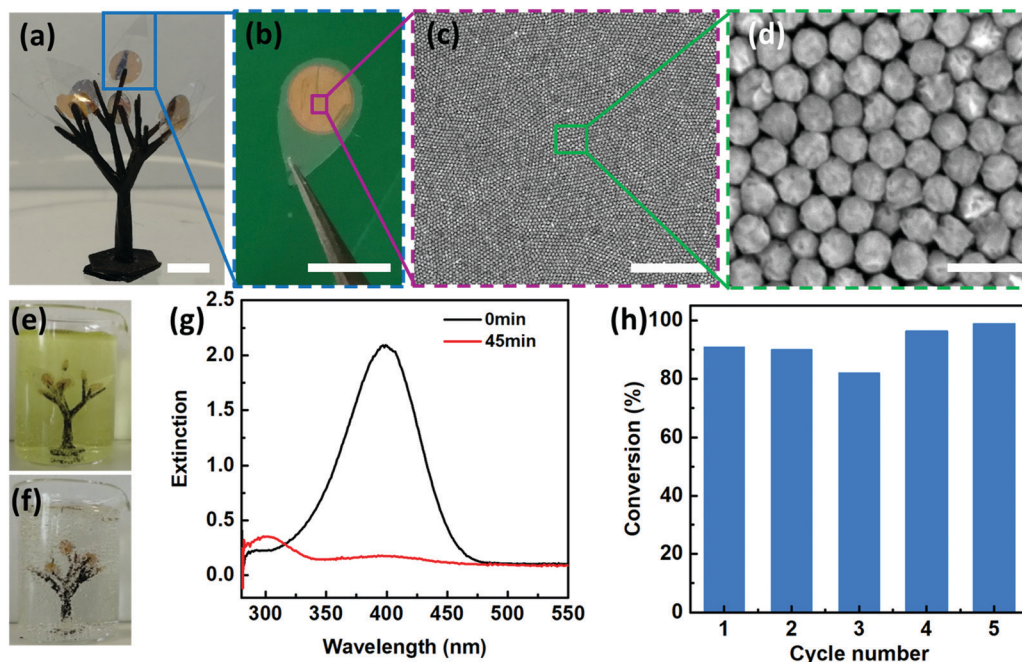

Fig. 5 An "artificial tree" built from the Janus plasmene. The photography of (a) the "artificial tree" (scale bar, 5 mm) and (b) an "artificial leaf" (scale bar, 5 mm). SEM images of a Janus plasmene nanosheet at (c) low (scale bar, 1 μm) and (d) high (scale bar, 100 nm) magnification. Photos of the reaction solution (e) before and (f) after reacting for 45 min. (g) The change in the UV-vis spectra of the catalytic reaction solution after reacting for 45 min using the "artificial tree". (h) Conversion efficiency of 4-NP in 5 cycles.

cell in a natural leaf, the underlying leaf-shaped flexible poly(ethylene terephthalate) (PET) is analogous to the epidermis in a natural leaf (Fig. 5b), and the 3D-printed frames correspond to the tree branches. We then immersed the "artificial tree" into water containing 4-NP (Fig. 5e). Remarkably, under sunlight irradiation, 8 pieces of leaves could successfully convert 30 mL of 4-NP solution to 4-AP within 45 min under sunlight irradiation (Fig. 5f and g and supporting video, ESI†). In contrast, the conversion could not be achieved in the absence of the "artificial tree" (Fig. S18, ESI†) under the same conditions. The "artificial tree" was highly durable and structurally stable during the entire photocatalytic reaction. It could be easily taken out and was ready for the next reaction in another beaker when the first reaction was finished, demonstrating the potential for continuous catalytic reactions similar to the way natural photosynthesis occurs. We found that the "artificial tree" showed no significant loss of conversion efficiency even after 5 cycles of reactions (Fig. 5h) or after one-year storage (Fig. S19, ESI†), indicating potential real-world applications in solar fuel production or contaminant degradation in a river.

Conclusions

In conclusion, we demonstrate a 2D flexible photocatalyst from a close packed Janus plasmene nanosheet with two distinct sides – one is hydrophilic catalytic Pd and another is hydrophobic plasmonic Au. The unique 2D Janus structure and functions could offer not only the capability of sunlight harvesting and efficiently converting solar to chemical energy but also stability in aqueous solutions without any dissolution or degradation. The 2D integration of catalytically active materials with a plasmonic nanostructure allows one to synthetically tune the photocatalytic performance by either optimizing the thickness of the catalytic component or controlling the structure of the plasmene nanosheets (*i.e.* the building block shape or their alignment). Furthermore, the Janus plasmene nanosheets could be used to construct a 3D "artificial tree", which successfully converted 30 mL of 4-NP to 4-AP in a continuous manner without regeneration of the catalysts, akin to the way a natural tree undertakes photosynthesis. The results presented here indicate the potential of our 2D Janus plasmene nanosheets in the design of tailor-made flexible photocatalysts for sustainable solar-to-chemical conversion.

Author contributions

R. Fu, Q. Shi and W. Cheng co-designed and conceived the experiments. R. Fu, Q. Shi and Z. Yong carried out the experimental work on the synthesis of nanoparticles, fabrication of plasmene nanosheets and characterization. J. C. Griffith carried out the XPS measurement and analysis. L. W. Yap 3D printed and spray painted the artificial tree. W. Cheng, R. Fu, Q. Shi, Z. Yong, J. C. Griffith and L. W. Yap analysed the experimental data and co-wrote the manuscript. All authors have given approval to the final version of the manuscript.

Conflicts of interest

There are no conflicts to declare.

Acknowledgements

Notes and references

1 M. Pelaez, N. T. Nolan, S. C. Pillai, M. K. Seery, P. Falaras, A. G. Kontos, P. S. Dunlop, J. W. Hamilton, J. A. Byrne and K. O'shea, *Appl. Catal., B*, 2012, **125**, 331–349.

2 H. Huang, L. Zhang, Z. Lv, R. Long, C. Zhang, Y. Lin, K. Wei, C. Wang, L. Chen and Z.-Y. Li, *J. Am. Chem. Soc.*, 2016, **138**, 6822–6828.

3 B. Li, T. Gu, T. Ming, J. Wang, P. Wang, J. Wang and J. C. Yu, *ACS Nano*, 2014, **8**, 8152–8162.

4 N. E. Motl, A. F. Smith, C. J. DeSantis and S. E. Skrabalak, *Chem. Soc. Rev.*, 2014, **43**, 3823–3834.

5 S. Kim, J. M. Kim, J. E. Park and J. M. Nam, *Adv. Mater.*, 2018, **30**, 1704528.

6 M. Rycenga, C. M. Cobley, J. Zeng, W. Li, C. H. Moran, Q. Zhang, D. Qin and Y. Xia, *Chem. Rev.*, 2011, **111**, 3669–3712.

7 M. Xiao, R. Jiang, F. Wang, C. Fang, J. Wang and J. C. Yu, *J. Mater. Chem. A*, 2013, **1**, 5790–5805.

8 C. Zhan, X.-J. Chen, J. Yi, J.-F. Li, D.-Y. Wu and Z.-Q. Tian, *Nat. Rev. Chem.*, 2018, **2**, 216–230.

9 Y. Mu, H. Zhang, W. Zheng and X. Cui, *New J. Chem.*, 2017, **41**, 786–792.

10 O. Guselnikova, A. Olshtrem, Y. Kalachyova, I. Panov, P. Postnikov, V. Svorcik and O. Lyutakov, *J. Phys. Chem. C*, 2018, **122**, 26613–26622.

11 Y. Qu, R. Cheng, Q. Su and X. Duan, *J. Am. Chem. Soc.*, 2011, **133**, 16730–16733.

12 Y. Hu, Y. Liu, Z. Li and Y. Sun, *Adv. Funct. Mater.*, 2014, **24**, 2828–2836.

13 Z. Zheng, T. Tachikawa and T. Majima, *J. Am. Chem. Soc.*, 2015, **137**, 948–957.

14 P. Christopher, H. Xin and S. Linic, *Nat. Chem.*, 2011, **3**, 467–472.

15 W. H. Hung, M. Aykol, D. Valley, W. Hou and S. B. Cronin, *Nano Lett.*, 2010, **10**, 1314–1318.

16 S. Sarina, H. Zhu, E. Jaatinen, Q. Xiao, H. Liu, J. Jia, C. Chen and J. Zhao, *J. Am. Chem. Soc.*, 2013, **135**, 5793–5801.

17 Q. Xiao, S. Sarina, E. Jaatinen, J. Jia, D. P. Arnold, H. Liu and H. Zhu, *Green Chem.*, 2014, **16**, 4272–4285.

18 W. Xiong, D. Sikdar, L. W. Yap, P. Guo, M. Premaratne, X. Li and W. Cheng, *Nano Res.*, 2016, **9**, 415–423.

19 S. T. Marshall, M. O'Brien, B. Oetter, A. Corpuz, R. M. Richards, D. K. Schwartz and J. W. Medlin, *Nat. Mater.*, 2010, **9**, 853–858.

20 J. Zhou, B. Duan, Z. Fang, J. Song, C. Wang, P. B. Messersmith and H. Duan, *Adv. Mater.*, 2014, **26**, 701–705.

21 D. Dong, R. Fu, Q. Shi and W. Cheng, *Nat. Protoc.*, 2019, **14**, 2691–2706.

22 K. J. Si, D. Sikdar, Y. Chen, F. Eftekhari, Z. Xu, Y. Tang, W. Xiong, P. Guo, S. Zhang, Y. Lu, Q. Bao, W. Zhu, M. Premaratne and W. Cheng, *ACS Nano*, 2014, **8**, 11086–11093.

23 Q. Shi, D. E. Gómez, D. Dong, D. Sikdar, R. Fu, Y. Liu, Y. Zhao, D.-M. Smilgies and W. Cheng, *Adv. Mater.*, 2019, **31**, 1900989.

24 P.-P. Fang, S. Duan, X.-D. Lin, J. R. Anema, J.-F. Li, O. Buriez, Y. Ding, F.-R. Fan, D.-Y. Wu, B. Ren, Z. L. Wang, C. Amatore and Z.-Q. Tian, *Chem. Sci.*, 2011, **2**, 531–539.

25 J. F. Moulder, W. F. Stickle, P. E. Sobol and K. D. Bomben, *Phys. Electron.*, 1995, 230–232.

26 M. C. Militello and S. J. Simko, *Surf. Sci. Spectra*, 1994, **3**, 387–394.

27 K. J. Si, Y. Chen, Q. Shi and W. Cheng, *Adv. Sci.*, 2018, **5**, 1700179.

28 J. He, W. Ji, L. Yao, Y. Wang, B. Khezri, R. D. Webster and H. Chen, *Adv. Mater.*, 2014, **26**, 4151–4155.

29 J. Zeng, Q. Zhang, J. Chen and Y. Xia, *Nano Lett.*, 2010, **10**, 30–35.

30 X. Kong, H. Zhu, C. Chen, G. Huang and Q. Chen, *Chem. Phys. Lett.*, 2017, **684**, 148–152.

31 M. J. Berr, P. Wagner, S. Fischbach, A. Vaneski, J. Schneider, A. S. Susha, A. L. Rogach, F. Jäckel and J. Feldmann, *Appl. Phys. Lett.*, 2012, **100**, 223903.

32 R. F. Steiner and E. P. Kirby, *J. Phys. Chem.*, 1969, **73**, 4130–4135.

33 X. Zhu, H. Jia, X.-M. Zhu, S. Cheng, X. Zhuo, F. Qin, Z. Yang and J. Wang, *Adv. Funct. Mater.*, 2017, **27**, 1700016.

34 H. Zhu, X. Ke, X. Yang, S. Sarina and H. Liu, *Angew. Chem., Int. Ed.*, 2010, **49**, 9657–9661.

35 E. Kazuma and Y. Kim, *Angew. Chem., Int. Ed.*, 2019, **58**, 4800–4808.

36 Z. Zhang, C. Zhang, H. Zheng and H. Xu, *Acc. Chem. Res.*, 2019, **52**, 2506–2515.

37 X. Zhang and Z. Su, *Adv. Mater.*, 2012, **24**, 4574–4577.

38 S. Sakthivel, M. V. Shankar, M. Palanichamy, B. Arabindoo, D. W. Bahnemann and V. Murugesan, *Water Res.*, 2004, **38**, 3001–3008.

39 T. A. G. Silva, E. Teixeira-Neto, N. López and L. M. Rossi, *Sci. Rep.*, 2014, **4**, 5766.

40 J.-W. Hu, J.-F. Li, B. Ren, D.-Y. Wu, S.-G. Sun and Z.-Q. Tian, *J. Phys. Chem. C*, 2007, **111**, 1105–1112.

41 Y. Xiang, X. Wu, D. Liu, X. Jiang, W. Chu, Z. Li, Y. Ma, W. Zhou and S. Xie, *Nano Lett.*, 2006, **6**, 2290–2294.

42 K. J. Si, D. Sikdar, L. W. Yap, J. K. K. Foo, P. Guo, Q. Shi, M. Premaratne and W. Cheng, *Adv. Opt. Mater.*, 2015, **3**, 1710–1717.

43 Q. Shi, K. J. Si, D. Sikdar, L. W. Yap, M. Premaratne and W. Cheng, *ACS Nano*, 2016, **10**, 967–976.

44 D. Dong, L. W. Yap, D. M. Smilgies, K. J. Si, Q. Shi and W. Cheng, *Nanoscale*, 2018, **10**, 5065–5071.

45 K. C. Ng, I. B. Udagedara, I. D. Rukhlenko, Y. Chen, Y. Tang, M. Premaratne and W. Cheng, *ACS Nano*, 2012, **6**, 925–934.